Electronic Supplementary Material (ESI) for Inorganic Chemistry Frontiers.

Supplementary Information

Efficient Electrochemical Coupling of Nitrate and Biomass-derived Acetone to Acetoxime at High Current Density over Zn/Cu Hexagonal Nanosheets Catalyst

Shao et al.

1. Experimental Section

Materials:

All reagents were commercially purchased. KNO_3, KNO_2, CH_3COCH_3, $(NH_4)_2S_2O_8$, NaOH, Na_2SO_4, $ZnCl_2$, $(CH_3)_2COH$, 5,5-dimethyl-1-pyrroline-N-oxide (DMPO) and dimethyl sulfoxide (DMSO) were all of analytical grade. The concentrations of H_2SO_4, HCl, NH_2OH, N_2H_4, and NH_3 were 98%, 36%, 50%, 80%, and 28%, respectively. Metal foils (1 cm x 2 cm x 0.1 mm) of Co, Fe, Ag, Zn, Pb, Sn, Pt, Ni, and Cu were purchased from Zhong Nuo Advanced Material (Beijing) Technology CO. All reagents were used without further purification. Deionized water was used in all experimental processes.

Material Synthesis:

Synthesis of $Cu(OH)_2$ nanowires ($Cu(OH)_2$NWs/CF):

Firstly, foam copper (CF) was pretreated by cutting it into 1 cm x 2 cm x 1 mm pieces. Then, it was sonicated for 3 minutes in 10% HCl, acetone, ethanol, and deionized water to remove surface contaminants. The cleaned CF was dried in a vacuum oven and then immersed vertically into alkaline oxidative etchant solution (AOES) containing 0.25 M $(NH_4)_2S_2O_8$ and 5 M NaOH for 15 minutes. The color of CF surface turned light blue, and after rinsing with deionized water, $Cu(OH)_2$ nanowires ($Cu(OH)_2$NWs/CF) were obtained[1, 2].

Synthesis of Cu nanowires (CuNWs/CF):

$Cu(OH)_2$NWS/CF was calcined in air at 220°C for two hours at a ramp rate of 5°C/min. Afterward, the color of material surface changed from blue to grey, named CuONWs/CF. Then in an H-type electrolytic cell with 0.5 M Na_2SO_4 as electrolyte, CuONWs/CF served as the working electrode, Pt and Ag/AgCl as the counter and reference electrodes, respectively, with an applied current density of -36 mA cm^{-2} for 45 minutes until the surface of the working electrode changed from light grey to red[3].

Synthesis of Zn/Cu hexagonal nanosheets (Zn/Cu/CF):

0.136g of $ZnCl_2$ powder was dissolved in 10 mL of deionized water under vigorous stirring for 5 minutes, resulting in a turbid solution (Solution A). The above-prepared $Cu(OH)_2$NWs/CF was then vertically immersed in Solution with mild stirring for immersion times of 3, 6, and 12 hours. Characterization before and after immersion indicated that $ZnCl_2$ underwent hydrolysis to form $Zn(OH)_2$ attached to $Cu(OH)_2$ nanowires, and structural rearrangement of $Cu(OH)_2$NWs occurred, transforming them into ultrathin nanosheets. After extraction and vacuum drying, $Zn(OH)_2/Cu(OH)_2$ nanosheets were obtained and named $Zn^{2+}/Cu(OH)_2$/CF-3/6/12 according to the immersion time. To stabilize Zn^{2+} on its surface, further calcination at 220°C in an air atmosphere yielded ZnO/CuO/CF- 3/6/12. Subsequent *in situ* electroreduction in a three-electrode system, as detailed for CuNWs/CF, resulted in Zn/Cu/CF-3/6/12.

Characterizations:

Powder X-ray diffraction (XRD) analysis was performed using a Rigaku D/MAX-2000 powder X-ray diffractometer with Cu Kα radiation. The scanning rate was 10 °C/min with an incident slit width of 1/2°.

Scanning electron microscopy (SEM) and corresponding energy dispersive X-ray spectroscopy (EDS) were conducted using a Hitachi S-4800 cold field emission scanning electron microscope. Samples were fixed on a sample holder with conductive adhesive and operated at 3 kV and 10 μA.

Transmission electron microscopy (TEM) analysis was carried out using a JEOL JEM-2100 instrument, with samples dispersed in ethanol, drop-cast onto carbon-coated copper grids, then air-

dried before testing. High-resolution TEM (HRTEM) and corresponding EDS were performed on a JEOL JEM-2100F instrument. Accelerating voltage was set to 200 kV.

X-ray photoelectron spectroscopy (XPS) was conducted using a Kratos Ultra X-ray photoelectron spectrometer with monochromatic Al Kα radiation. Samples were pressed onto Al foil and analyzed with the C1s peak at 284.8eV for calibration.

Inductively coupled plasma optical emission spectrometry (ICP-OES) was performed by digesting samples in aqua regia and 30% hydrogen peroxide, and diluting to proper volume before testing.

Electrochemical measurements:

All electrochemical tests were conducted using a Wuhan Corrtest Instruments Co., Ltd electrochemical workstation in an H-type electrolytic cell. Metal catalyst screening experiments were performed using metal foil sheets (1 cm x 2 cm x 0.1 mm) as the working electrode, with Pt mesh, and Hg/HgO as the counter and reference electrodes, respectively. 0.5M KOH with added 0.2 M acetone and 0.2 M potassium nitrate was used as electrolyte, and cathodic and anodic chambers were separated by a Nafion 117 membrane. Electrolyte volumes were both 30mL, and a current density of -100 mA cm^{-2} was applied for 2 hours. In order to screen the electrolyte pH, 0.5 M KOH was replaced with 0.1 M H_2SO_4 and 0.25 M K_2SO_4, while maintaining 0.5 M KOH as the electrolyte, and the nitrate concentration was optimized subsequently. The performance of the CuNWs/CF, Zn, Zn/Cu/CF-3, Zn/Cu/CF-6 and Zn/Cu/CF-12 was evaluated at different current densities (-20 to -200 mA cm^{-2}) under optimal pH and nitrate concentrations.

Linear sweep voltammetry (LSV) was conducted with a potential range of -0.5063~-1.6063 V vs Hg/HgO and a scan rate of 10 mV s^{-1} over different catalysts and electrolytes.

Cyclic voltammetry (CV) was performed with a potential range of ±50 mV vs open circuit potential and a scan rate of 20-120 mV s^{-1}.

Product identification and quantification:

The C-containing liquid products were firstly confirmed by 400 MHz ^{1}H-nuclear magnetic resonance (^{1}H NMR), further confirmed using gas chromatography (GC) by extraction of the post-reaction solution with ethyl acetate (EA). Additionally, the post-reaction solution was subjected to 600 MHz ^{13}C nuclear magnetic resonance (^{13}C-NMR) analysis, and the formation of the target product, acetone oxime, was confirmed by comparison with standard samples. Quantification of the C-containing liquid products was performed using ^{1}H NMR, with DMSO used as an internal standard[4]. After testing, neutralization was carried out with 50 sccm CO_2 until the pH approaching 8. Subsequently, 0.5 mL of the post-reaction solution and 0.1 mL of internal standard solution were mixed, and the internal standard solution was prepared as follows: (1) 10μL of dimethyl sulfoxide (DMSO) was diluted to 100 mL to prepare solution A; (2) Mix equal volumes of solution A and D_2O to obtain the internal standard solution. A standard curve was established based on the ratio of the peak areas of standard samples to the internal standard peak area and the concentration of the standard samples for quantitative analysis of C-containing liquid products. UV-vis absorption spectroscopy colorimetric tests were used to quantitatively analyze nitrogen-containing by-products such as NH_4^+, NO_2^-, and NH_2OH.

The quantitative method for NH_4^+ detection was conducted using the indophenol method[5, 6]. The colorimetric reagent preparation involved initially preparing Solution A by dissolving 50g L^{-1} sodium salicylate, 50g L^{-1} potassium sodium tartrate, and 20g L^{-1} sodium hydroxide in water. Solution B consisted of 10g L^{-1} nitroprusside, and Solution C comprised of 40 mL L^{-1} sodium

phosphate, 13%wt sodium hypochlorite (NaClO), and 30g L^{-1} sodium hydroxide. After the reaction, the solution was diluted 250 times. 5mL of the sample was mixed with 0.5ml of Solution A, 0.05ml of Solution B, and 0.05mL of Solution C, followed by a 20 minutes incubation. The absorbance was then measured at 650 nm. A standard curve was established using NH_4Cl crystals, dried at 105°C for 2 hours in advance, to prepare standard solutions ranging from 0 to 50μM.

For NO_2^- quantification[7], the colorimetric reagent was prepared by dissolving 20g of p-aminobenzenesulfonamide in 250mL of deionized water, followed by the addition of 50mL of phosphoric acid. After sonication and complete dissolution, 1g of N-(1-naphthyl)-ethylenediamine dihydrochlorid was added to the solution, and the volume was adjusted to 500 mL to obtain the NO_2^- colorimetric reagent. For testing, 5mL of the 250-fold diluted post-reaction solution was mixed with the reagent, incubated for 20 minutes, and the absorbance was measured at 540 nm. Standard solutions were prepared at concentrations ranging from 0 to 50 μM.

Similarly, a colorimetric method was employed for NH_2OH quantification[8]. The reagent for NH_2OH was prepared by diluting 1mL of the electrolyte with an equal volume of 0.05 M phosphate buffer (pH = 6.8) and 0.8 mL of deionized water to obtain Solution D. Solution E was prepared by diluting 1M Na_2CO_3 with deionized water, and Solution F was prepared by dissolving 0.007 M 8-hydroxyquinoline in ethanol. One milliliter each of Solutions E and F, and 0.2mL of trichloroacetic acid were added to Solution D. After incubation, the mixture was boiled in a water bath for 1 minute under dark conditions. The absorbance was then measured at 705 nm to establish a standard curve based on the relationship between absorbance values and concentrations.

The Faradaic efficiency (FE), yield rate, and selectivity (C) of the products were calculated as follows:

$$FE\ (\%) = C_i \times Z_i \times V \times F / Q \times 100\%$$

Where C_i represents the concentration of the product after the reaction, Zi represents the number of electrons transferred per molecule of synthesized product (6 for acetone oxime, 2 for isopropanol, 8 for ammonia, 2 for NO_2^- and 6 for NH_2OH), V represents the volume of the reaction solution, F is Faradaic constant (96485 C mol^{-1}), and Q is the total coulombs consumed in the reaction.

$$\text{Yield rate} = \mu mole\ of\ product / (reaction\ time \times area)$$

Where area represents the catalyst area immersed in the electrolyte.

$$\text{Selectivity (C)} = mole\ of\ acetoxime / mole\ of\ consumed\ acetone \times 100\%.$$

GC-MS:

GC-MS was performed on a GCMS-QP2020 NX, before the GC-MS test, acetoxime was extracted from the post-electrolyte using ethyl acetate, the extracted solution was then injected into GC-MS system for analysis.

ATR-IRAS:

In situ electrochemical attenuated total reflectance-infrared absorption spectroscopy (ATR-IRAS) mmeasurements were performed using a Bruker Vertex 70 instrument equipped with a liquid nitrogen-cooled mercury cadmium telluride (MCT) detector. The electrochemical *in situ* infrared cell and accessories were obtained from LingLu Instruments (Shanghai). The infrared cell was made of polyether ether ketone (PEEK), and the infrared prism window was made of transparent CaF_2. The catalyst was dispersed in ethanol, drop-casted onto a glassy carbon electrode, and tested with Ag/AgCl and Pt wire as the reference and counter electrodes, respectively[9]. The working electrode distance from the CaF_2 crystal window was controlled within 10 μm using a micrometer for

capturing the signals of intermediates. The Zn/Cu/CF-6 electrode was tested before and after the addition of acetone using a CS350MA electrochemical workstation, with background spectra collected at open circuit potential and potentials applied in the range of 0.4 to -0.4V vs RHE.

DEMS:

Online electrochemical differential mass spectrometry (DEMS) measurements were performed using a LingLu instruments system equipped with a CS350MA electrochemical workstation to detect small molecule volatile substances during real-time reaction processes. The molecules were collected via molecular pump vacuum through a hydrophobic polytetrafluoroethylene (PTFE) membrane, which played a crucial role in allowing small molecule volatilization while preventing water from entering the vacuum chamber. The electrolytic reaction occurred on one side of the PTFE membrane, and the volatile small molecules generated were pumped to the other side and detected sequentially by a mass spectrometer. The Zn/Cu/CF-6 electrode was cut to an appropriate size, pressed under a glassy carbon electrode, and used as the working electrode, with Pt wire and Ag/AgCl as the counter and reference electrodes, respectively. The current was alternately set to -50 mA cm^{-2} and 0, and the signal changes of key intermediates during current on/off were tested, with each measurement repeated more than three times.

Quasi *in situ* EPR:

Quasi *in situ* electron paramagnetic resonance (EPR) trapping of hydrogen and carbon radicals was performed on a Bruker A300, with Zn/Cu/CF as the working electrode, and Pt and Hg/HgO as the counter and reference electrodes, respectively. The reaction was conducted at -150 mA cm^{-2} for five minutes, with 0.1 mM DMPO trapping agent added during the reaction. Subsequently, the solution near the electrode was collected for EPR testing.

2. Additional results and discussion

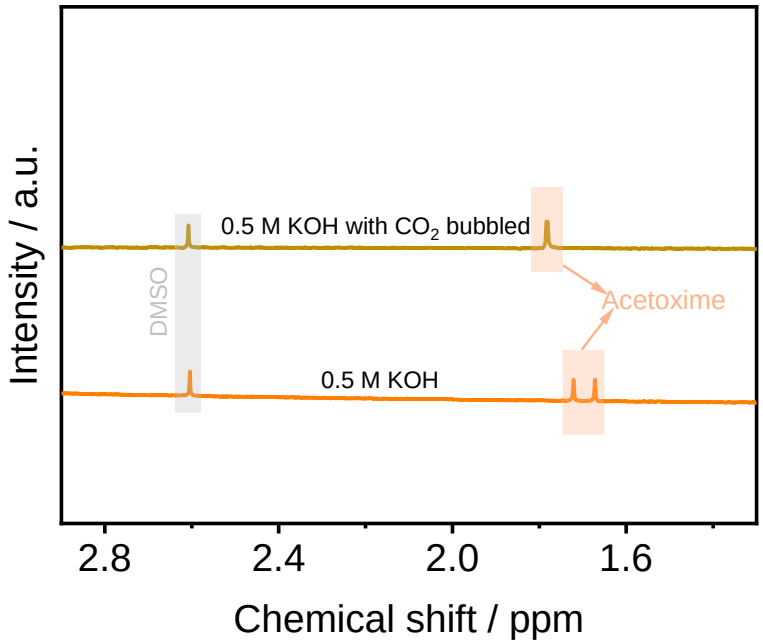

Figure S1. ^{1}H NMR spectrum of 75 ppm acetoxime in 0.5 M KOH solution and 0.5 M KOH with CO_2 bubbled.

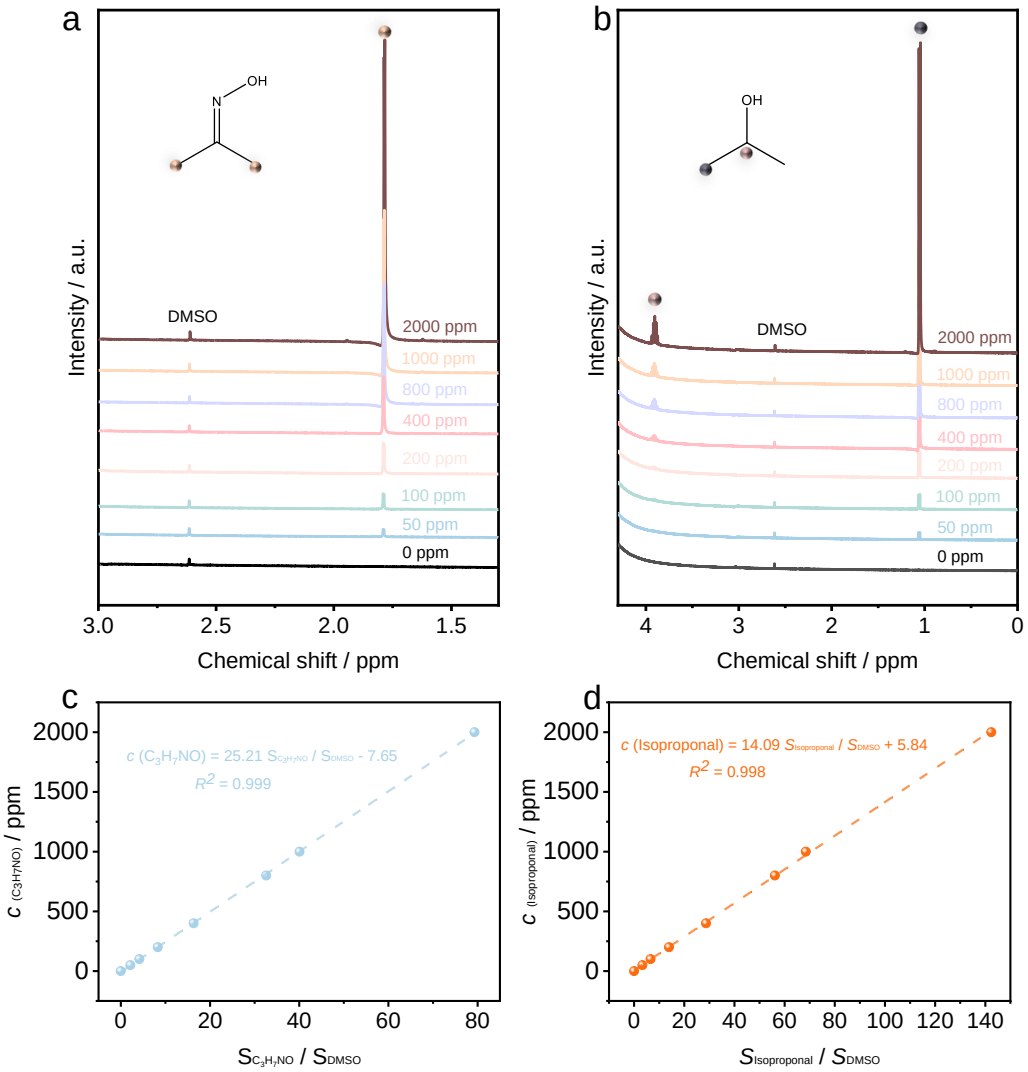

Figure S2. The concentration-dependent ^{1}H NMR spectra of (a) acetoxime and (b) isopropanol. (c) Linear calibration curve of the ratio of the peak area of acetoxime to that of the internal standard DMSO vs. the concentration of acetoxime, (d) linear calibration curve of the ratio of the peak area of isopropanol to that of the internal standard DMSO vs. the concentration of isopropanol.

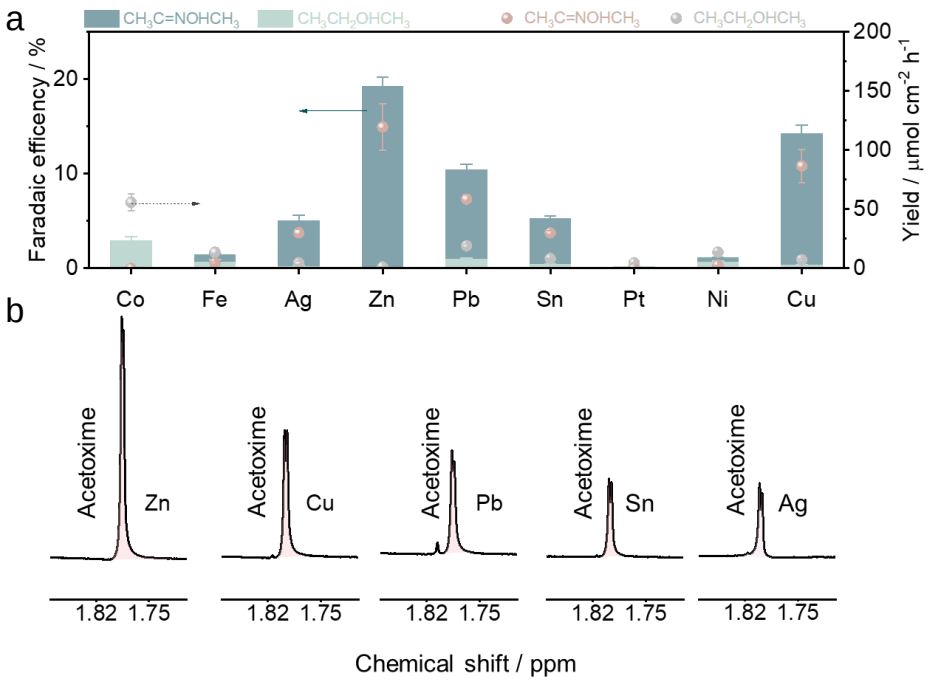

Figure S3. (a) Faradaic efficiency and yield rate of acetoxime and isopropanol over different metal catalysts. (b) ^{1}H NMR spectra of acetoxime electrosynthesis over Zn, Cu, Pb, Sn and Ag electrocatalysts.

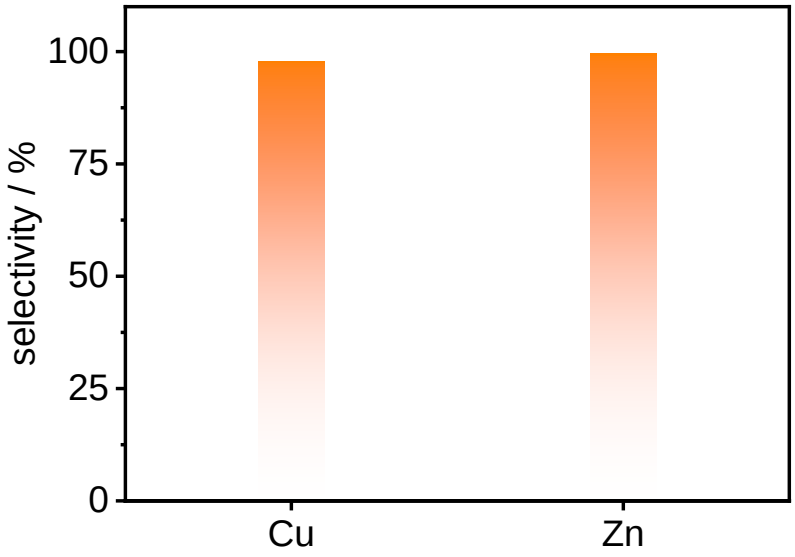

Figure S4. C selectivity of acetoxime for Cu and Zn electrocatalysts considering carbon containing products only as acetoxime and isopropanol.

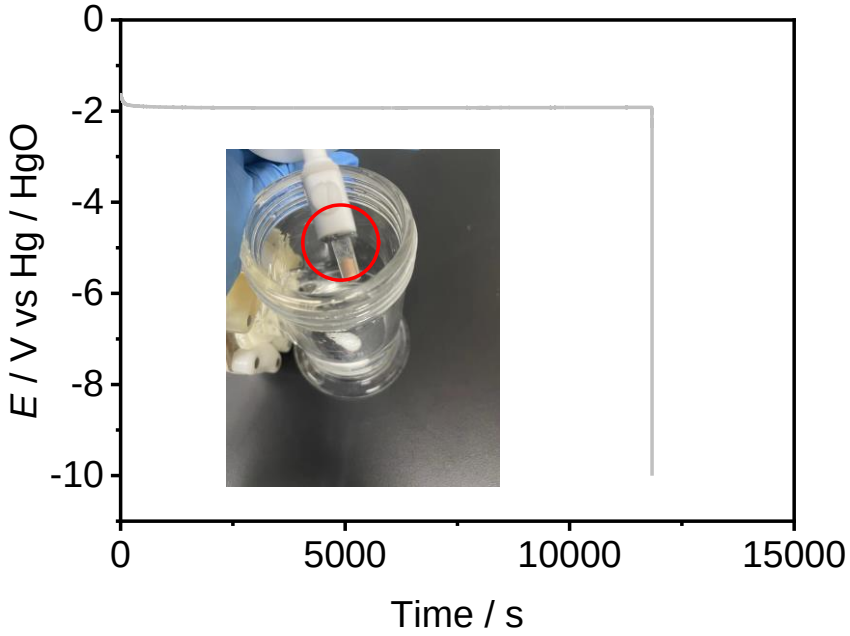

Figure S5. Potential-time curve of Zn at -100 mA cm^{-2} and image of used Zn electrode (red circle).

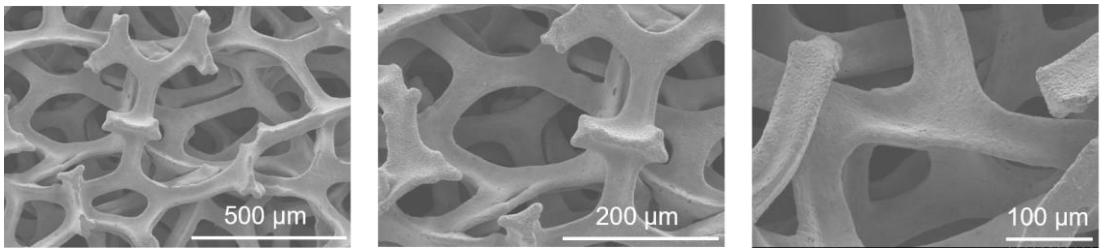

Figure S6. SEM images of Cu foam.

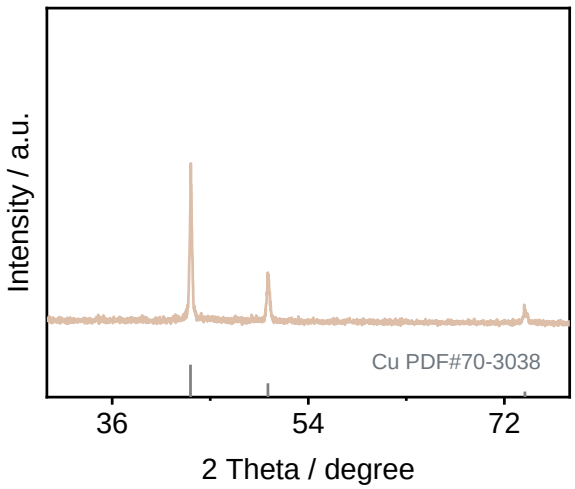

Figure S7. XRD pattern of Cu foam.

Figure S8. Images of cleaned Cu foam and $Cu(OH)_2$ NWs/CF.

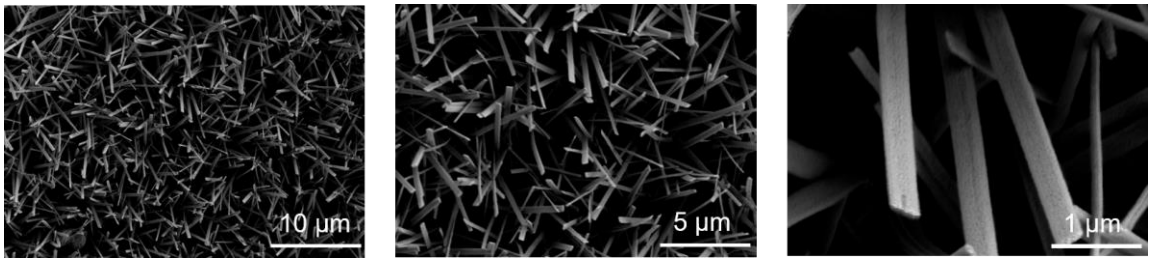

Figure S9. SEM images of $Cu(OH)_2$ NWs/CF.

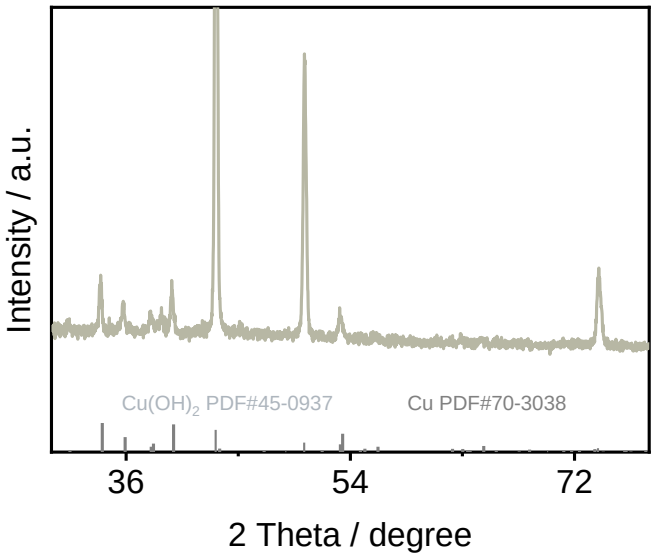

Figure S10. XRD pattern of $Cu(OH)_2$ NWs/CF.

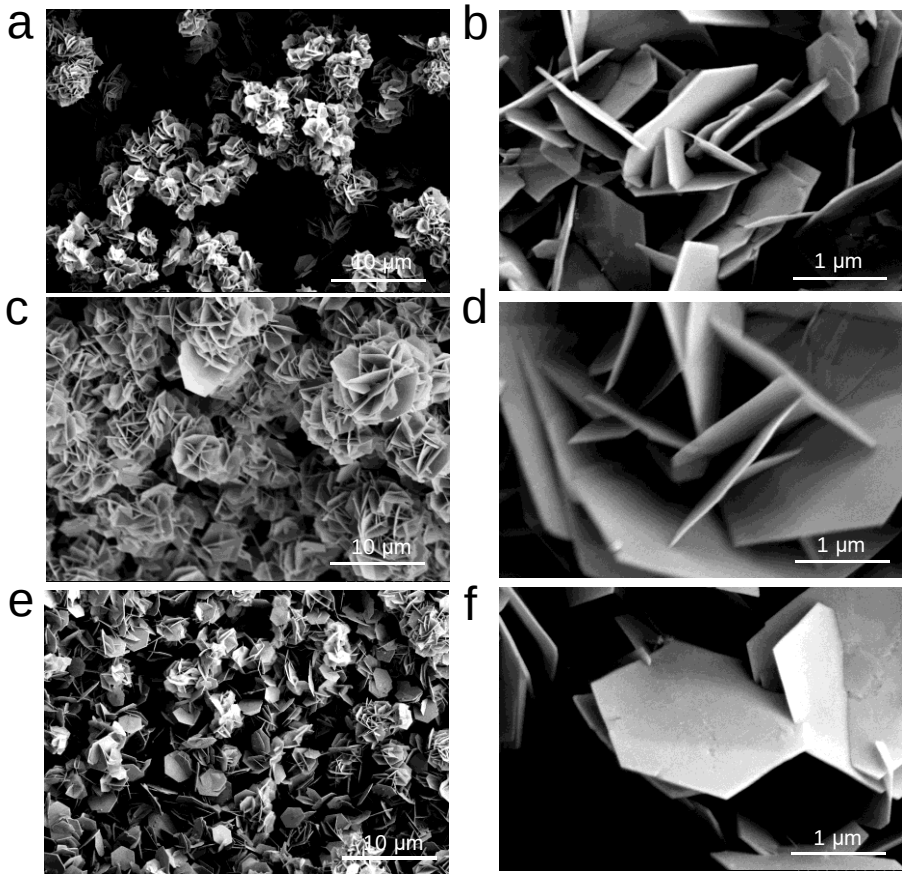

Figure S11. SEM images of (a-b) $Zn^{2+}/Cu(OH)_2$/CF-3, (c-d) $Zn^{2+}/Cu(OH)_2$/CF-6, (e-f) $Zn^{2+}/Cu(OH)_2$/CF-12 at different magnifications.

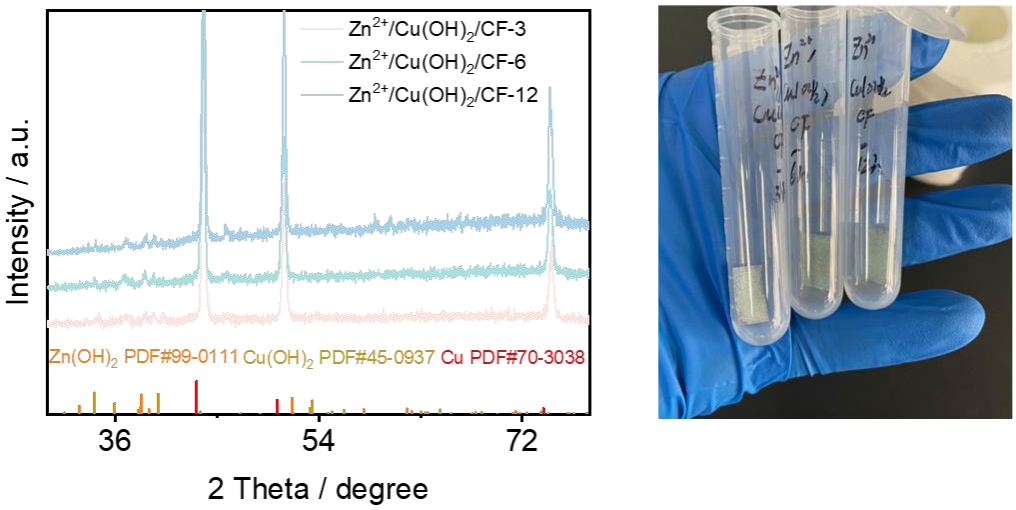

Figure S12. XRD patterns and image of $Zn^{2+}/Cu(OH)_2/CF$.

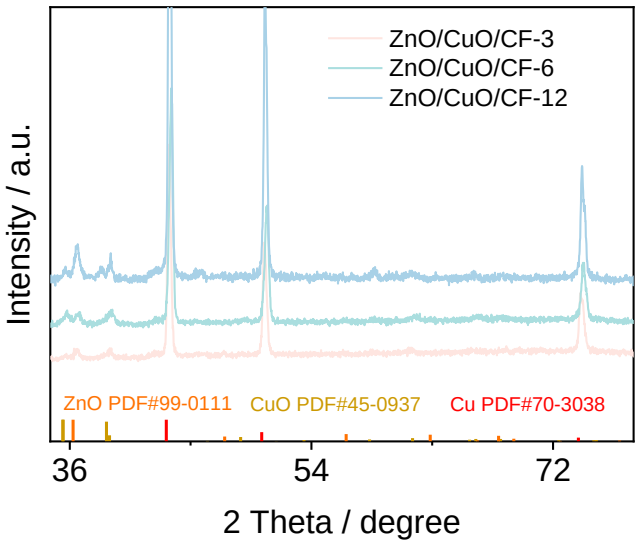

Figure S13. XRD patterns of ZnO/CuO/CF-3、ZnO/CuO/CF-6、ZnO/CuO/CF-12.

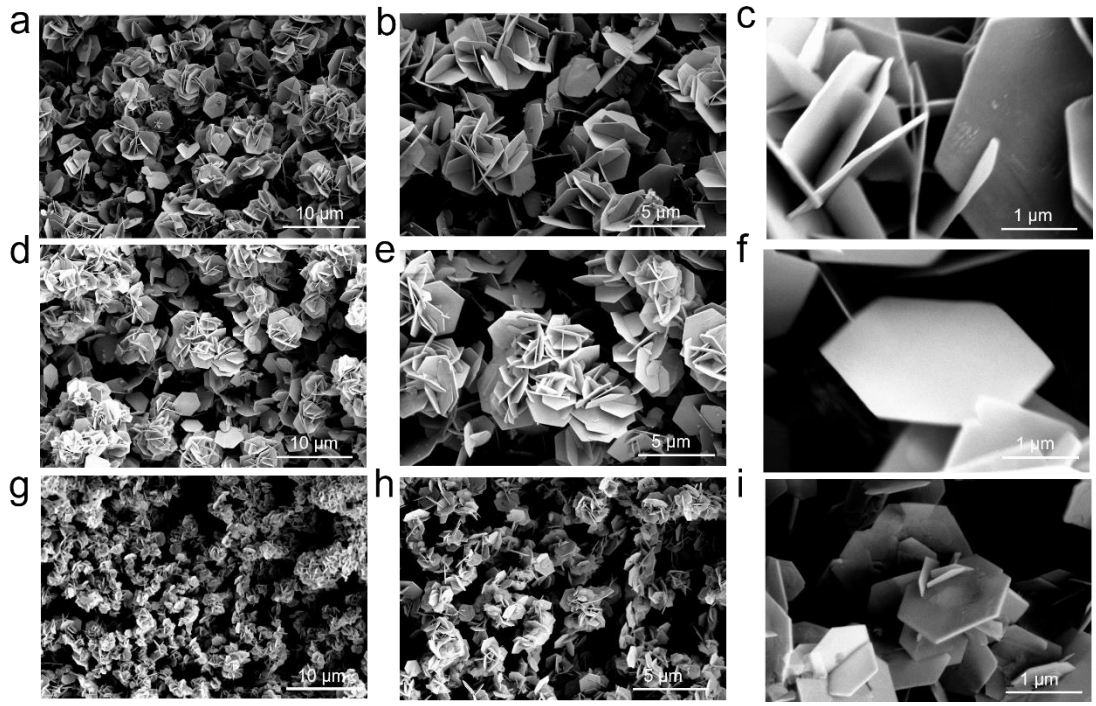

Figure S14. SEM images of (a-c) ZnO/CuO/CF-3, (d-f) ZnO/CuO/CF-6, (g-i) ZnO/CuO /CF-12 at different magnifications.

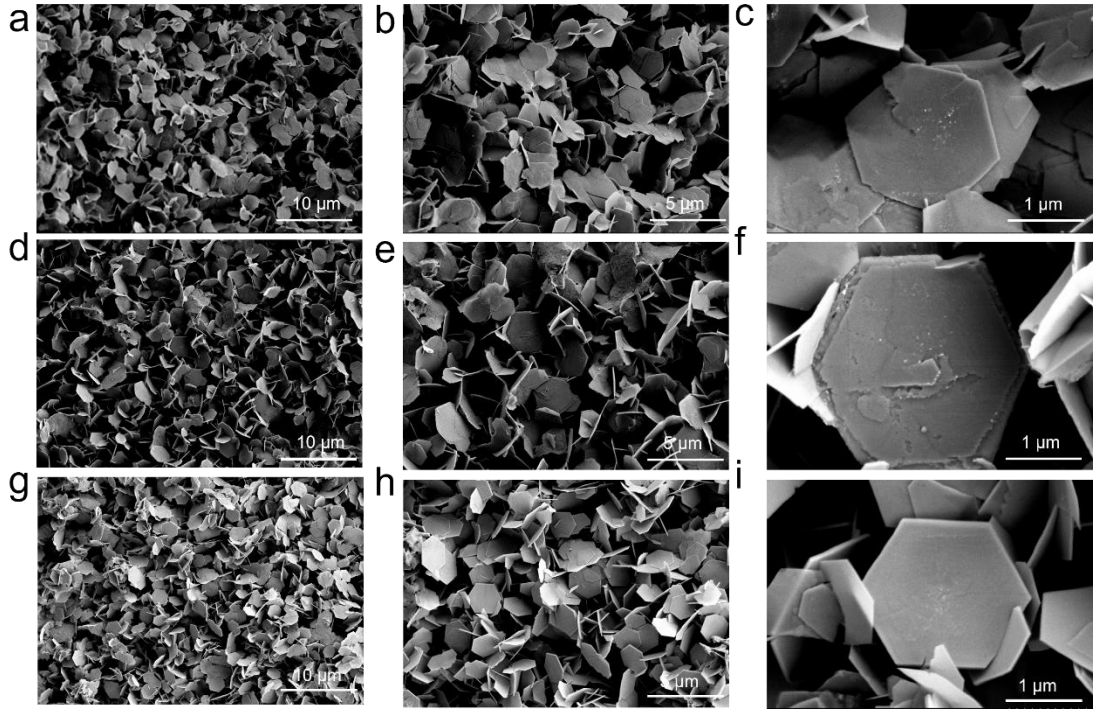

Figure S15. SEM images of (a-c) Zn/Cu/CF-3, (d-f) Zn/Cu/CF-6, (g-i) Zn/Cu/CF-12 at different magnifications.

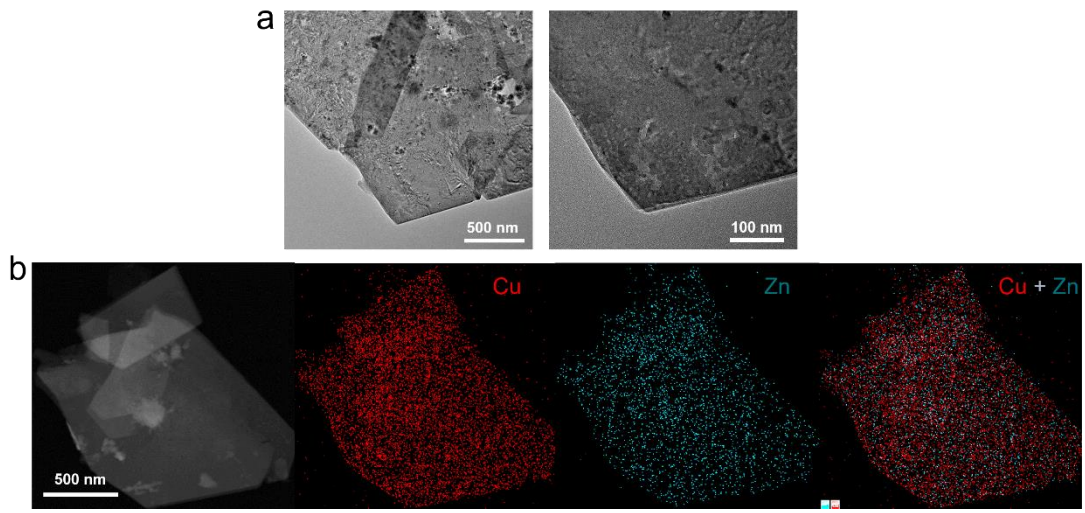

Figure S16. (a) TEM images of Zn/Cu/CF-6 and (b) corresponding EDS images of Zn and Cu elements.

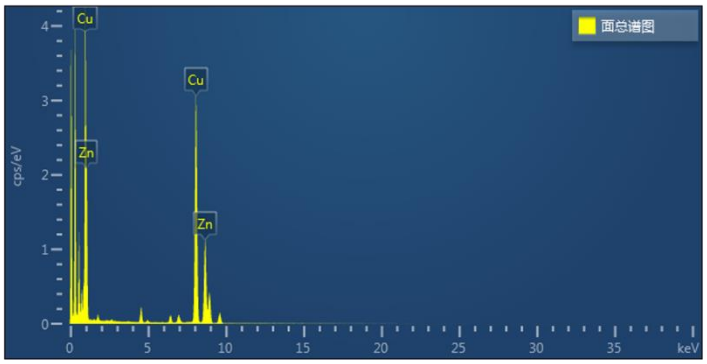

Element	wt%
Zn	19.52
Cu	80.48

Figure S17. TEM mapping of Zn and Cu over Zn/Cu/CF-6.

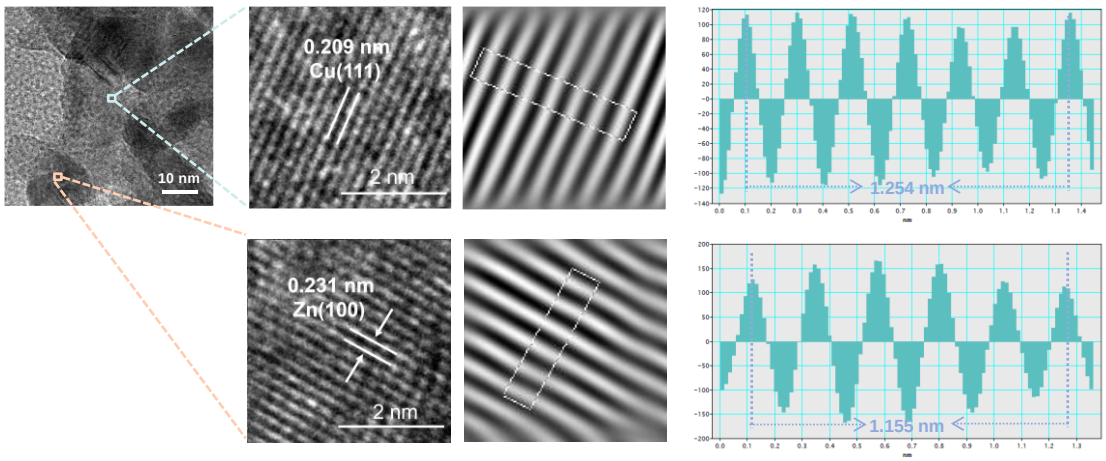

Figure S18. Lattice planes of Cu(111) and Zn(100).

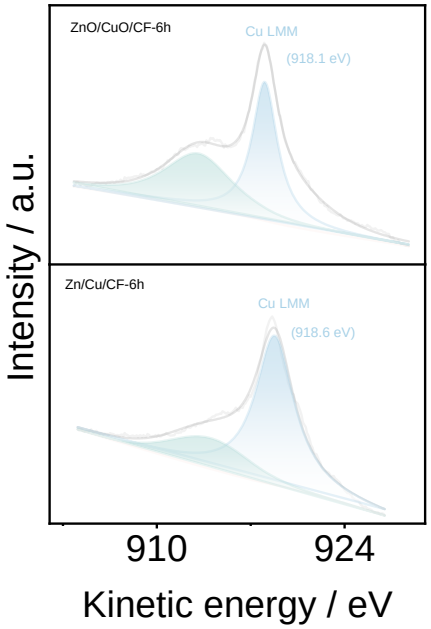

Figure S19. Cu LMM spectra of ZnO/CuO/CF-6, Zn/Cu/CF-6.

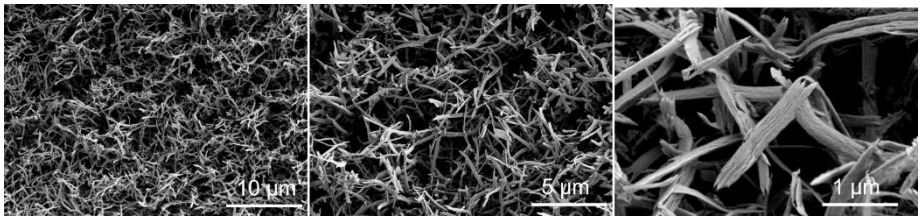

Figure S20. SEM images of CuO NWs/CF at different magnifications.

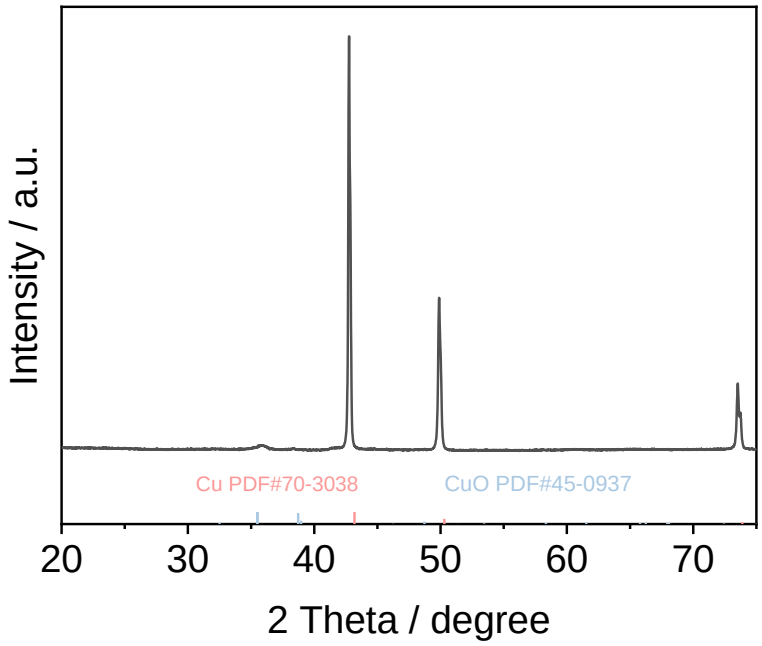

Figure S21. XRD pattern of CuO NWs/CF.

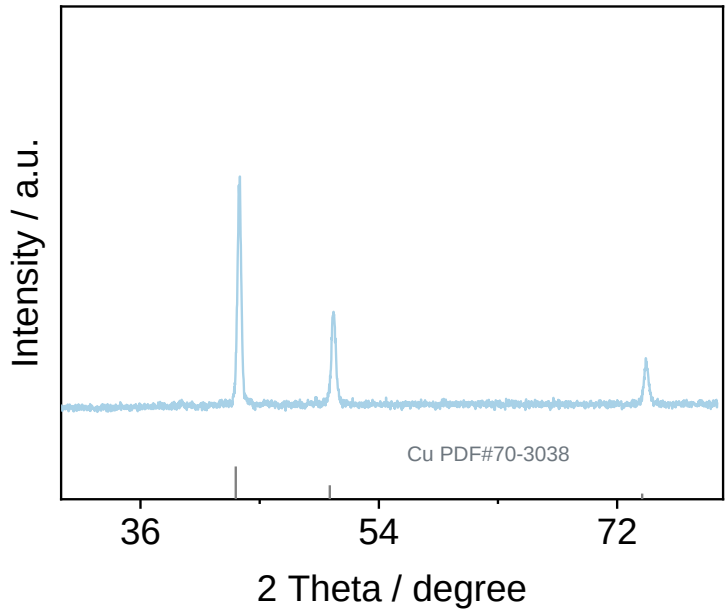

Figure S22. XRD pattern of CuNWs/CF.

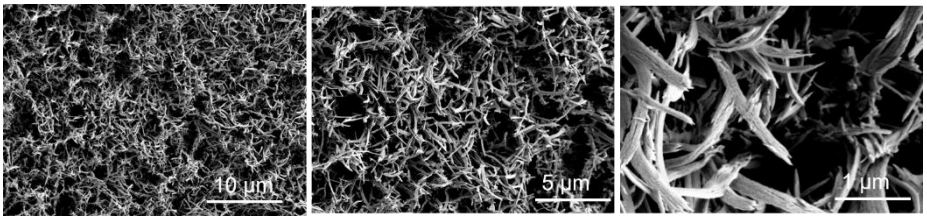

Figure S23. SEM images of CuNWs/CF at different magnifications.

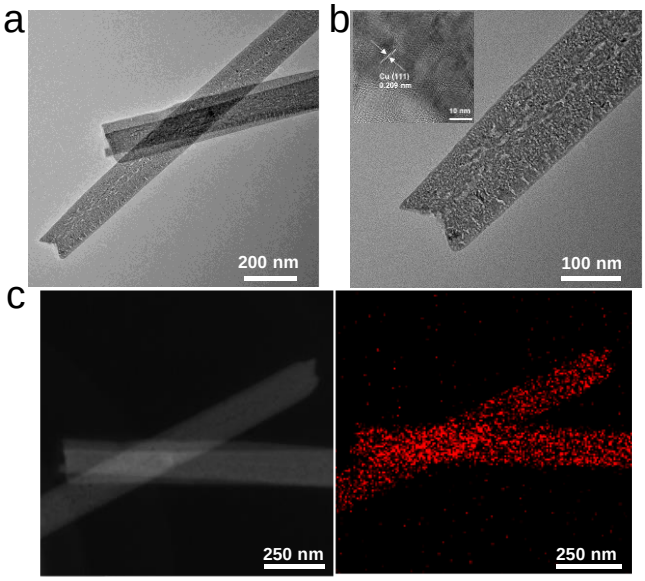

Figure S24. (a) TEM image of CuNWs/CF. (b) HRTEM image of CuNWs/CF. (c) TEM image and corresponding EDS of CuNWs/CF.

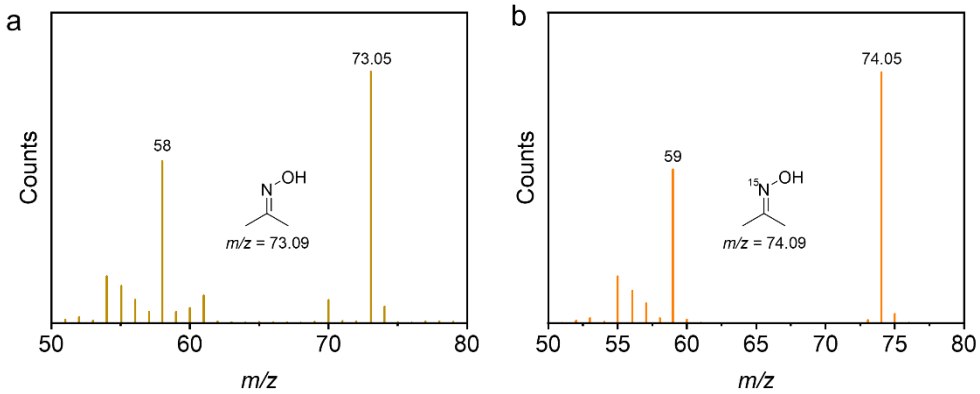

Figure S25. GC-MS detection for acetoxime and ^{15}N-labeled acetoxime.

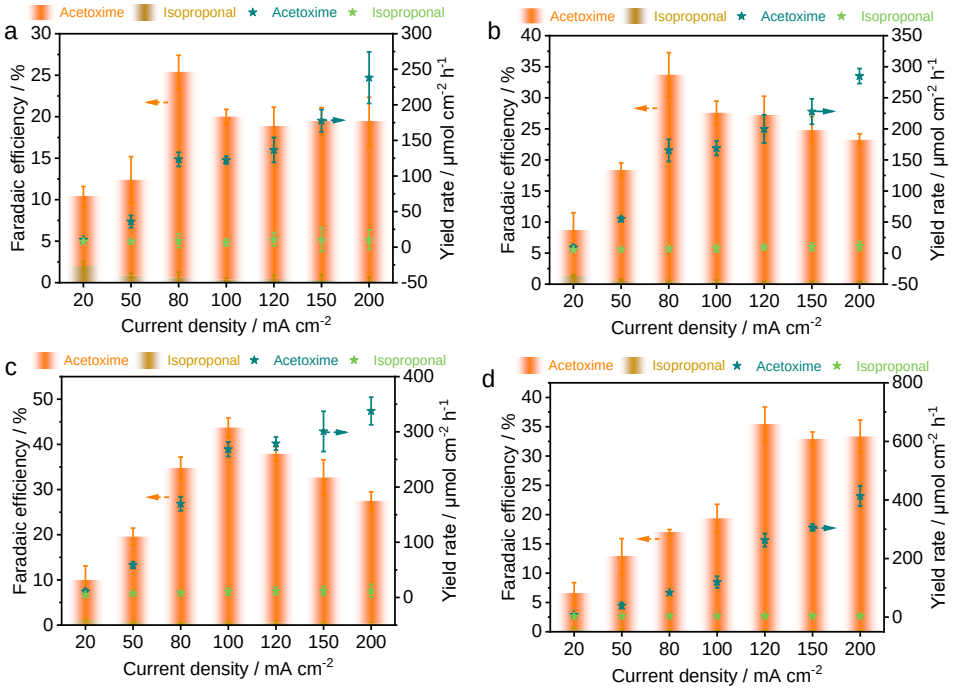

Figure S26. The current-dependent Faradaic efficiency and yield rate of carbon-containing liquid products over (a) CuNWs/CF, (b) Zn/Cu/CF-3, (c) Zn/Cu/CF-12, (d) Zn.

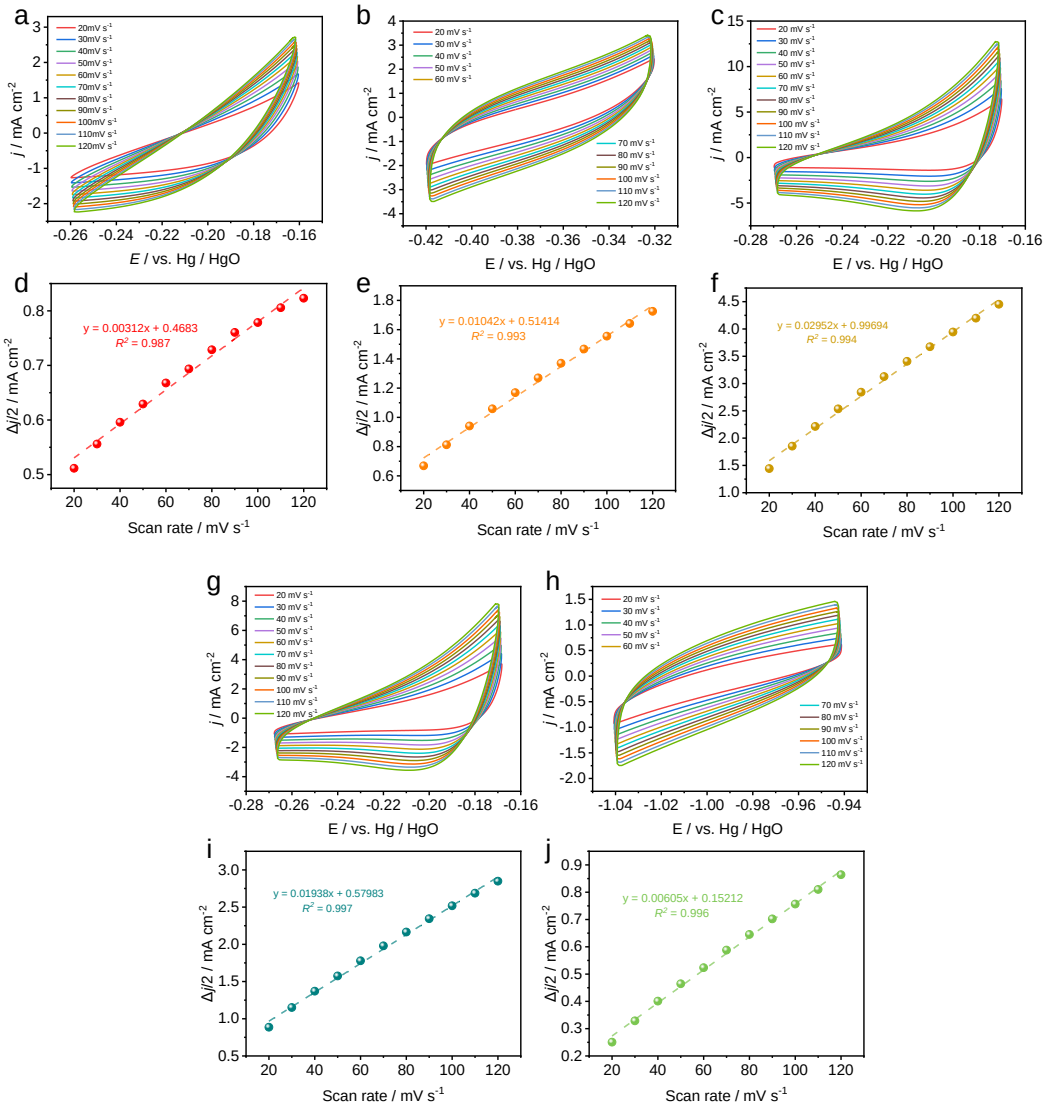

Figure S27. CV curves of (a) CuNWs/CF, (b) Zn/Cu/CF-3, (c) Zn/Cu/CF-6, (g) Zn/Cu/CF-12, (h)Zn at different scan rates from 20 to 120 mV s^{-1}. Fitting curves of $\Delta j/2$ (mA cm^{-2}) and scan rate(mV s^{-1}) of (d) CuNWs/CF, (e) Zn/Cu/CF-3, (f) Zn/Cu/CF-6, (i) Zn/Cu/CF-12, (j) Zn.

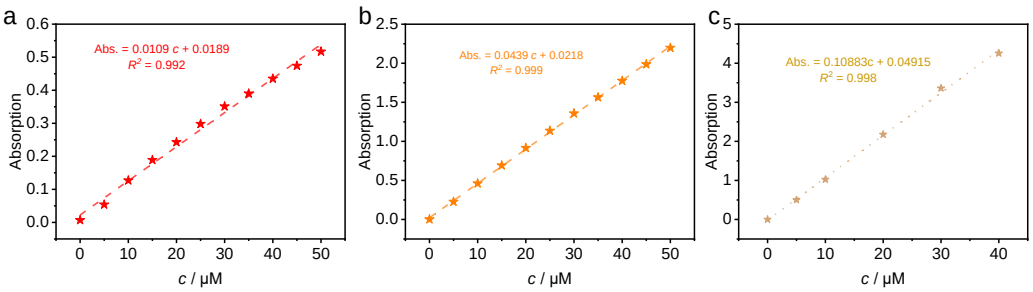

Figure S28. The linear relationship between absorbance values and concentration at a specific wavelength (NH_4^+~650 nm, NO_2^-~540 nm, NH_2OH~705 nm) of (a) NH_3, (b) NO_2^-, (c) NH_2OH.

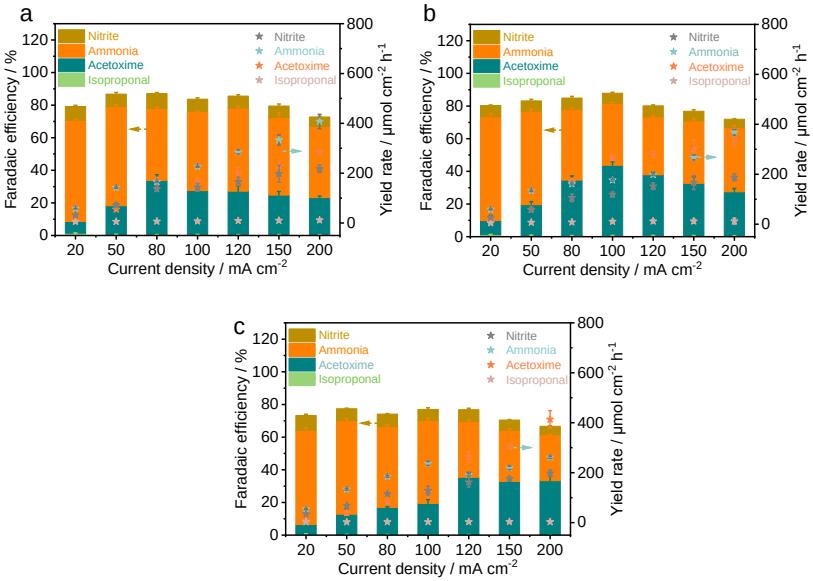

Figure S29. The current-dependent performance of (a) Zn/Cu/CF-3, (b) Zn/Cu/CF-12, (c) Zn.

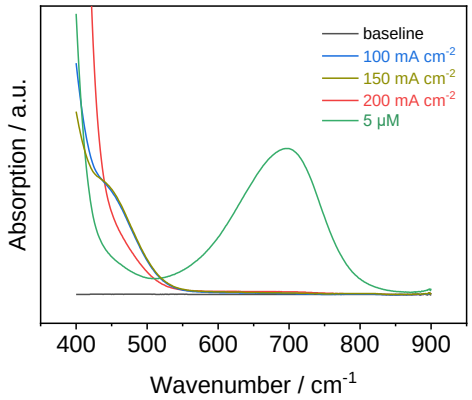

Figure S30. UV-vis absorption spectra of NH_2OH under different current densities.

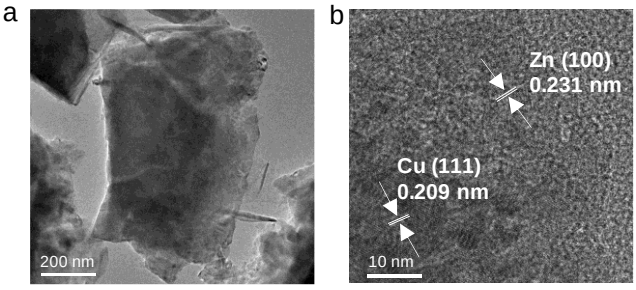

Figure S31. (a) TEM and (b) HRTEM images of Zn/Cu/6 after stability test.

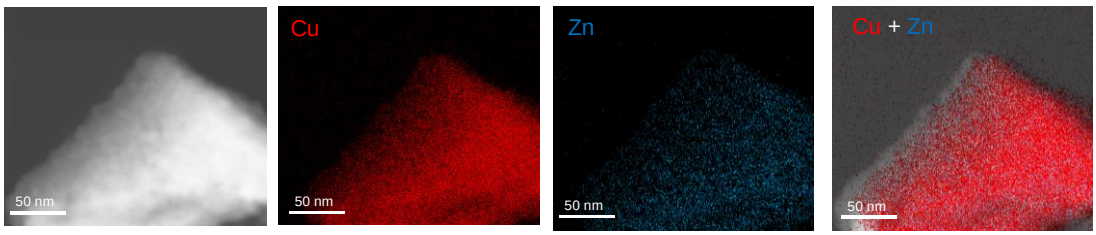

Figure S32. TEM and corresponding EDS images of Zn/Cu/CF-6 after stability test.

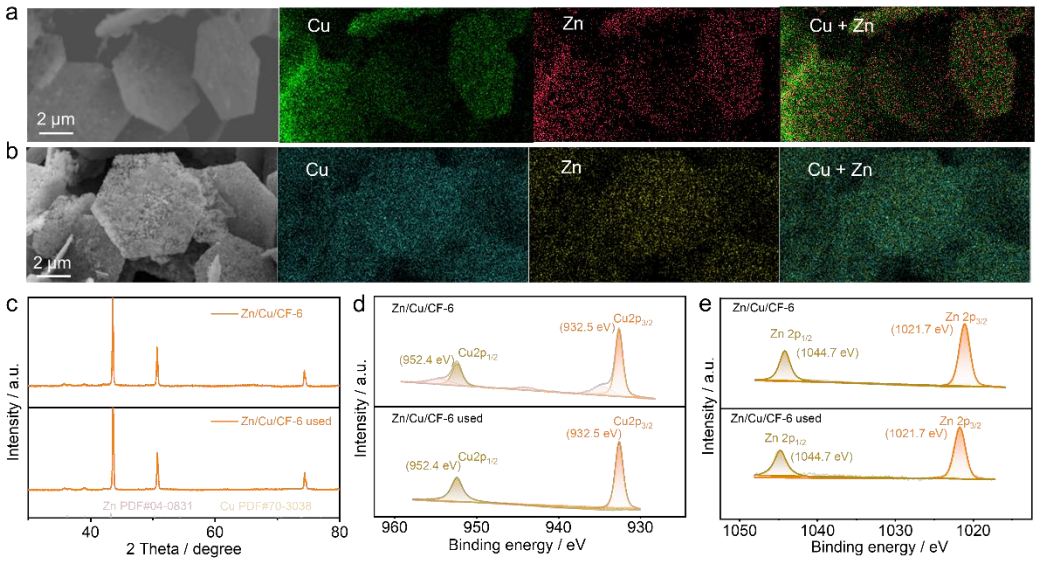

Figure S33. SEM and corresponding EDS mapping of Zn/Cu/CF-6 before (a) and after (b) stability test. (c) XRD patterns of Zn/Cu/CF-6 before and after stability test. Cu2p (d) and Zn2p (e) XPS results before and after stability test.

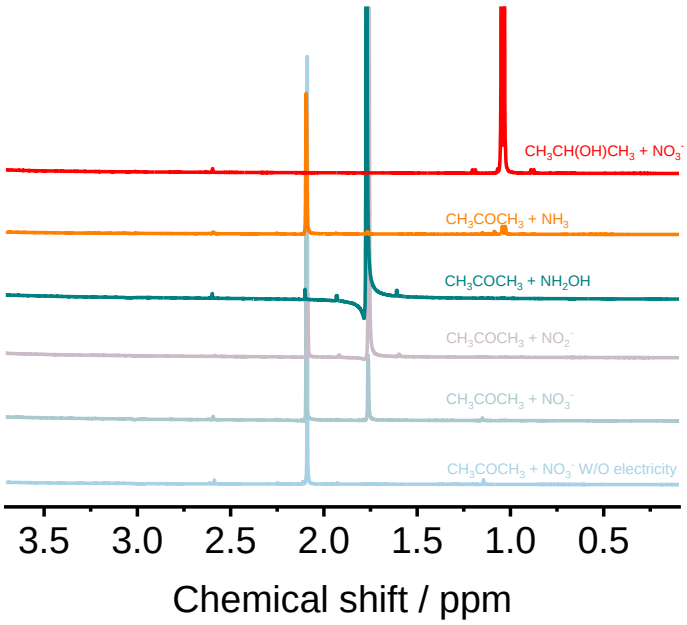

Figure S34. ^{1}H NMR spectra of electrolyte before reaction and electrolysis for 2 hours at -150 mA cm^{-2} of different carbon/nitrogen feedstocks.

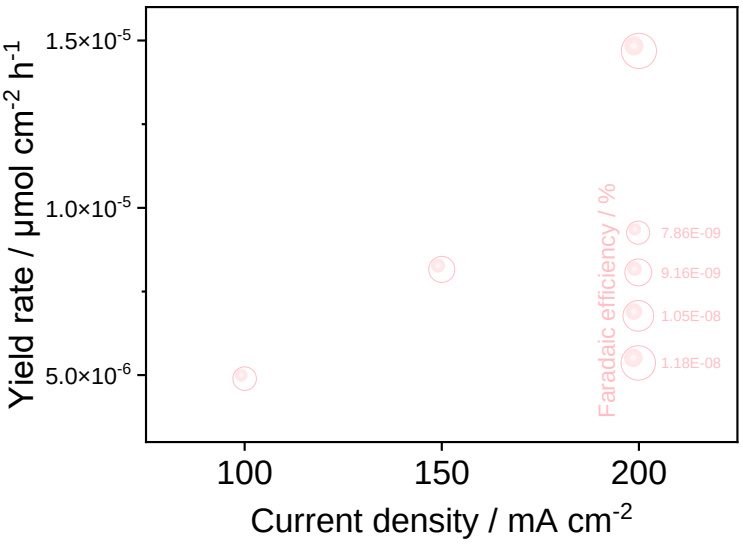

Figure S35. FE and yield rate of NH_2OH under different current densities.

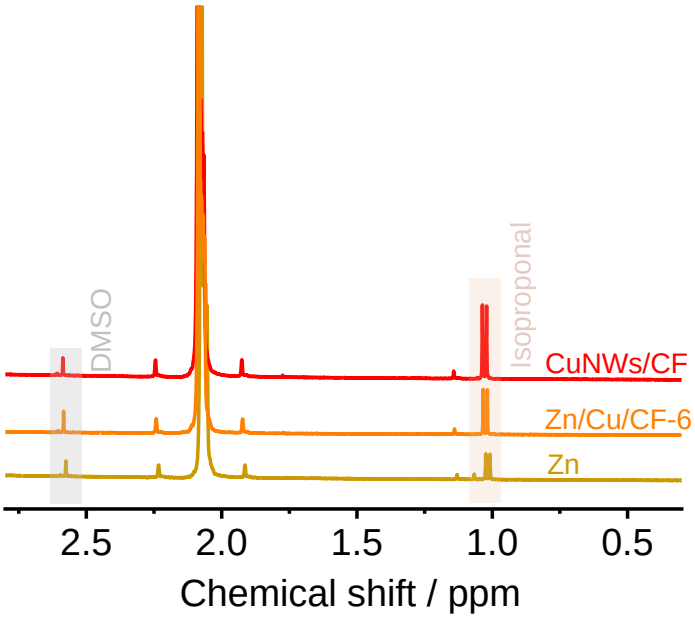

Figure S36. ^1H NMR spectra of Zn/Cu/CF-6, CuNWs/CF, Zn for e-ARR.

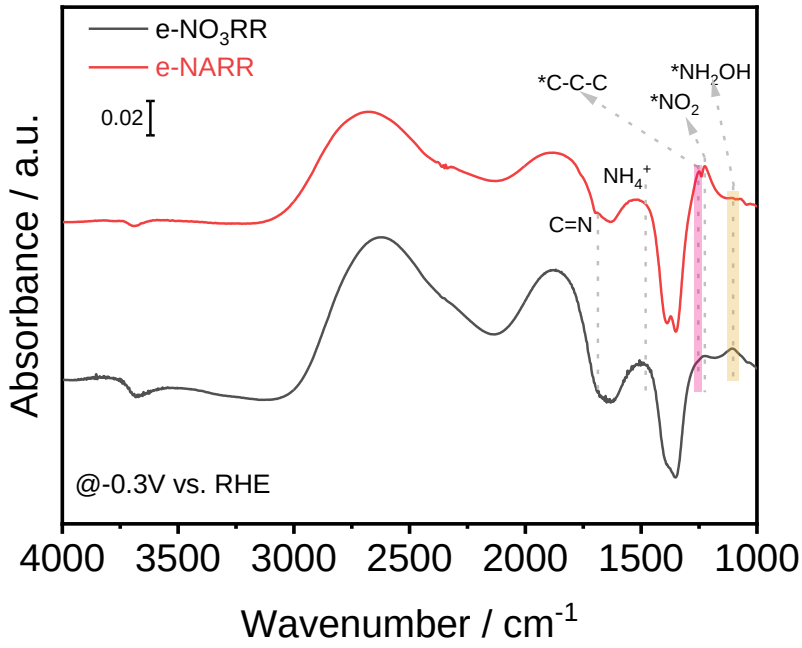

Figure 37. *in situ* ATR-IRAS of e-NO_3RR and e-NARR over Zn/Cu/CF-6 catalyst at -0.3 V vs. RHE.

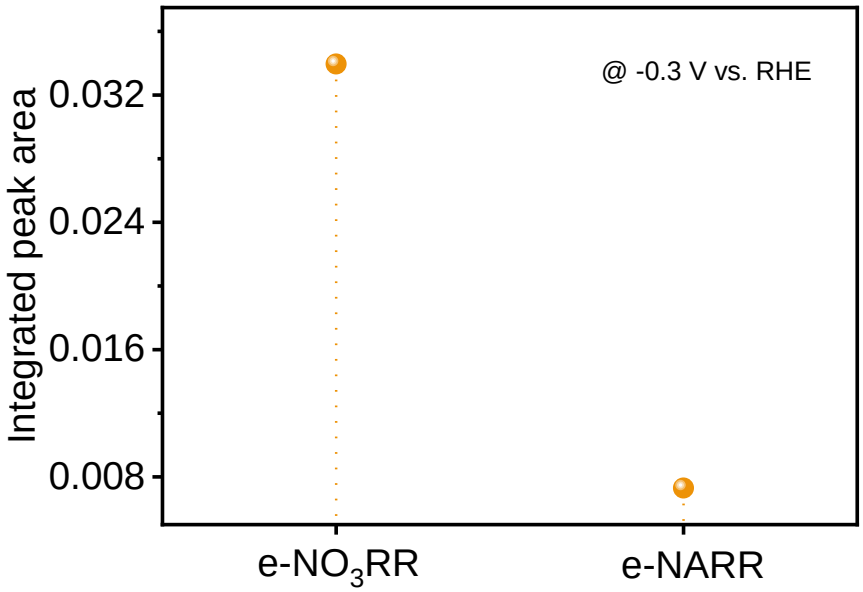

Figure 38. Integrated peak area of $^{*}NH_2OH$ from *in situ* ATR-IRAS at -0.3 V vs. RHE.

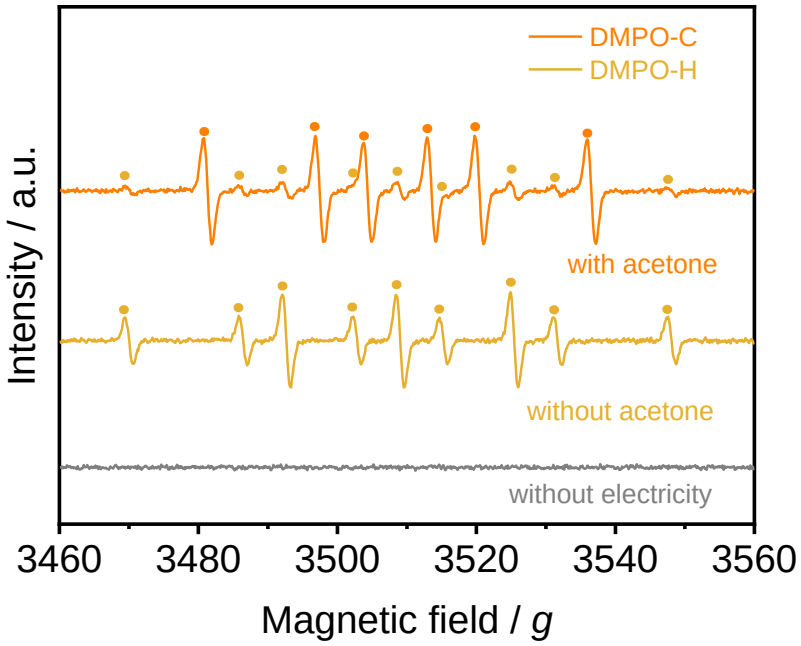

Figure 39. Quasi *in situ* electron paramagnetic resonance (EPR) trapping of hydrogen and carbon radicals over Zn/Cu/CF-6.

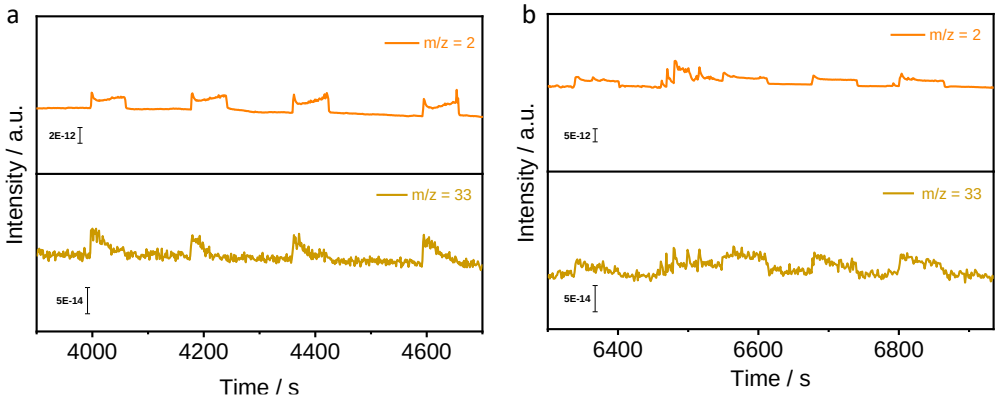

Figure S40. DEMS results of Zn/Cu/CF-6 for (a) e-NO_3RR and (b) e-NARR.

Table S1: ICP results of Zn/Cu/CF-3, Zn/Cu/CF-6, Zn/Cu/CF-12.

Sample	Zn%	Cu%
Zn/Cu/CF-3h	2.46	89.4
Zn/Cu/CF-6h	2.70	87.6
Zn/Cu/CF-12h	2.78	87.1

Table S2: Performance summary on oximes electrosynthesis from carbon/nitrogen-containing small molecules in recent three years.

References	Faradaic efficiency / %	Current density / mA cm^{-2}	Yield	Oximes and the corresponding feedstocks
This work	**44.5**	**150**	**415.5 μmol cm^{-2} h^{-1}**	**Acetoxime from nitrate and acetone**
ACS Catal. **2024**, 14, 3287–3297	27	100	167.9 μmol cm^{-2} h^{-1}	Cyclohexanone oxime from nitrate and cyclohexanone
Chem. Sci., **2023**, 14, 13198-13204	51.4	56	20.1 mg cm^{-2} h^{-1}	Cyclohexanone oxime from nitrate and cyclohexanone
Chem Catalysis, **2022**, 2, 1807–1818	44.8	22	10.7 mg cm^{-2} h^{-1}	Cyclohexanone oxime from NO and cyclohexanone
J. Am. Chem. Soc. **2024**, 146, 10934–10942	47.8	100	34.9 mg cm^{-2} h^{-1}	Cyclopentanone oxime from nitrate and cyclopentanone
J. Am. Chem. Soc. **2024**, 146, 6294–6306	37.2	30	22.8 g g_{cat}^{-1} h^{-1}	Benzaldoxime from NO_x and Benzaldehyde
Sci. China. Chem., **2023**, 66, 1758-1762	40.92	100	251 μmol cm^{-2} h^{-1}	Formaldoxime from nitrate and formaldehyde
	10.78	/	222 μmol cm^{-2} h^{-1}	Acetoxime from nitrate and acetone
Angew. Chem. Int. Ed. **2023**, 62, e202305491	20.1	/	55.9 g g_{cat}^{-1} h^{-1}	Cyclohexanone oxime from nitrate and cyclohexanone
Nat. Commun., **2023**, doi: 10.1038/s41467-023-38888-6	26	20	168 μmol cm^{-2} h^{-1}	Cyclopentanone oxime from nitrite and cyclopentanone
Angew. Chem. Int. Ed. **2023**, 62, e202312239	49.8	13	281 mg L^{-1} h^{-1}	pralidoxime from nitrite and pralidehyde

Table S3: The double-layer capacitance (C_{dl}) and corresponding electrochemical active surface area (ECSA) of different electrocatalysts.

Sample	C_{dl} / mF cm^{-2}	ECSA (C_s = 60 μF cm^{-2})
Cu NWs/CF	3.1	51.7
Zn/Cu/CF-3	10.4	173.3
Zn/Cu/CF-6	29.5	491.7
Zn/Cu/CF-12	19.4	323.3
Zn	6.1	101.7

Table S4: List of control experiments with different carbon/ nitrogen sources to infer the pathway of acetoxime electrosynthesis from NO_3^- and CH_3COCH_3.

Entry	C source	N source	Current density / mA cm^{-2}	Time / h	Acetoxime?
1	$(CH_3)_2CO$	NO_3^-	150	2	Yes (FE = 44.5%)
2	$(CH_3)_2CO$	NO_2^-	150	2	Yes (FE = 58.2%)
3	$(CH_3)_2CO$	N_2	150	2	No
4	$(CH_3)_2CO$	NH_2OH	150	2	Yes (Yield rate = 2.17 mmol cm^{-2} h^{-1})
5	$(CH_3)_2CO$	NH_3	150	2	No
6	$(CH3)_2COH$	NO_3^-	150	2	No
7	$(CH_3)_2CO$	NO_3^-	0	2	No

3. References

1. Y. Zhong, R. Ren, Y. Peng, J. Wang, X. Ren, Q. Li and Y. Fan, In situ construction of hierarchical Ag-decorated Cu nanowire arrays as an efficient and durable electrocatalyst for hydrogenation of 5-hydroxymethylfurfural and furfural, *Mol. Catal.*, 2022, **528**, 112487.
2. F.-Y. Chen, Z.-Y. Wu, S. Gupta, D. J. Rivera, S. V. Lambeets, S. Pecaut, J. Y. T. Kim, P. Zhu, Y. Z. Finfrock and D. M. Meira, Efficient conversion of low-concentration nitrate sources into ammonia on a Ru-dispersed Cu nanowire electrocatalyst, *Nat. Nanotechnol.*, 2022, **17**, 759-767.
3. W. Zhang, Y. Qi, Y. Zhao, W. Ge, L. Dong, J. Shen, H. Jiang and C. Li, Rh-dispersed Cu nanowire catalyst for boosting electrocatalytic hydrogenation of 5-hydroxymethylfurfural, *Sci. Bull.*, 2023, **68**, 2190-2199.
4. K. P. Kuhl, E. R. Cave, D. N. Abram and T. F. Jaramillo, New insights into the electrochemical reduction of carbon dioxide on metallic copper surfaces, *Energy Environ. Sci.*, 2012, **5**, 7050-7059.
5. Y. Wang, L. Zhang, Y. Niu, D. Fang, J. Wang, Q. Su and C. Wang, Boosting NH_3 production from nitrate electroreduction via electronic structure engineering of Fe_3C nanoflakes, *Green Chem.*, 2021, **23**, 7594-7608.
6. T. Muthusamy, S. S. Markandaraj and S. Shanmugam, Nickel nanoparticles wrapped in N-doped carbon nanostructures for efficient electrochemical reduction of NO to NH_3, *J. Mater. Chem. A*, 2022, **10**, 6470-6474.
7. E. Murphy, Y. Liu, I. Matanovic, S. Guo, P. Tieu, Y. Huang, A. Ly, S. Das, I. Zenyuk and X. Pan, Highly durable and selective Fe-and Mo-based atomically dispersed electrocatalysts for nitrate reduction to ammonia via distinct and synergized NO_2^- pathways, *ACS Catal.*, 2022, **12**, 6651-6662.
8. Q. Hu, K. Yang, O. Peng, M. Li, L. Ma, S. Huang, Y. Du, Z.-X. Xu, Q. Wang and Z. Chen, Ammonia Electrosynthesis from Nitrate Using a Ruthenium–Copper Cocatalyst System: A Full Concentration Range Study, *J. Am. Chem. Soc.*, 2023, **146**, 668-676.
9. X. Li, J. H. Wang, C. Y. Yuan, Q. W. Sun, J. Shao, X. C. Li, Z. L. Feng, H. Dong, C. Li and Y. W. Zhang, A Unique Amorphous Porous $BiSbO_x$ Nanotube with Abundant Unsaturated Sb-Stabilized BiO_{8-x} Sites for Efficient CO2 Electroreduction in a Wide Potential Window, *Adv. Funct. Mater.*, 2024, 2402220.